Discovery of a diamond-based photonic crystal structure in beetle scales

Jeremy W. Galusha,[1] Lauren R. Richey,[1,2] John S. Gardner,[2] Jennifer N. Cha,[3] and Michael H. Bartl[1,4,*]

[1]*Department of Chemistry, University of Utah, 315 South 1400 East, HEB Room 2020, Salt Lake City, Utah 84112, USA*
[2]*Department of Biology, Brigham Young University, 401 WIDB, Provo, Utah 84602, USA*
[3]*IBM Almaden Research Center, 650 Harry Road, San Jose, California 95120, USA*
[4]*Department of Physics, University of Utah, Salt Lake City, Utah 84112, USA*

We investigated the photonic crystal structure inside iridescent scales of the weevil *Lamprocyphus augustus*. By combining a high-resolution structure analysis technique based on sequential focused ion beam milling and scanning electron microscopy imaging with theoretical modeling and photonic band-structure calculations, we discovered a natural three-dimensional photonic structure with a diamond-based crystal lattice operating at visible wavelengths. Moreover, we found that within individual scales, the diamond-based structure is assembled in the form of differently oriented single-crystalline micrometer-sized pixels with only selected lattice planes facing the scales' top surface. A comparison of results obtained from optical microreflectance measurements with photonic band-structure calculations reveals that it is this sophisticated microassembly of the diamond-based crystal lattice that lends *Lamprocyphus augustus* its macroscopically near angle-independent green coloration.

Photonic structure engineering—the design and fabrication of periodically ordered dielectric composites with periodicities at optical wavelengths—has become an intense research field, since the realization of the potential impact of photonic band-structure concepts [1–3] on all-optical information processing [4]. Among the various photonic architectures, diamond-based lattices are the clear "champions" [5]. However, despite promising proposals [5–8] and successful fabrication progress in the infrared regime [9–12], a synthetic diamond-based photonic crystal with periodicities at visible wavelengths has not been realized. Here we report on a natural diamond-based photonic crystal operating in the visible. Employing a high-resolution three-dimensional (3D) structure analysis technique combined with theoretical modeling, we discovered that the brilliant green iridescence of the weevil *Lamprocyphus augustus* arises from exoskeleton scales with an interior diamond-based cuticular structure. Moreover, each single scale is composed of an array of differently oriented single-crystalline micrometer-sized domains, resulting in a macroscopic near angle-independent coloration.

Optical interference produced by the interaction of light with periodically ordered low and high refractive index structures is a widely used method in nature to produce intense iridescence colors. Especially, many species of Coleoptera and Lepidoptera have developed a wealth of cuticular exoskeleton photonic crystals with, for example, gyroid-like, tetrahedral-like, opal-like, and honeycomb-like structures, resulting in a variety of optical effects [13–16]. Figure 1(a) shows the deep green colored weevil *L. augustus*. In contrast to typical multilayer and opal-like natural photonic structures with strongly angle-dependent iridescence colors, this weevil possesses—even at highly oblique angles—a

near angle-independent coloration, hinting at an elaborate multidomain photonic structure [15]. Optical microscopy studies show that this near angle-independent iridescence originates from individual leaflike shaped cuticle scales attached to the beetle's exoskeleton [Fig. 1(b)]. Given the relatively low refractive index of cuticular chitin-based material, the presence of a near angle-independent coloration points to highly efficient 3D photonic structure engineering.

To investigate the origin of the green iridescence of *L. augustus* the internal cuticular structure was examined by cross-sectional scanning electron microscopy (SEM) imaging of individual scales embedded into a low viscosity resin [Fig. 1(c)]. A glass knife in combination with an ultramicrotome was used to perform random cross-sectional cuts, which were imaged with an FEI XL30 ESEM/FEG electron microscope. Each scale seems to be composed of seemingly different looking domains of unique crystalline features such as the layered "sheets" of hexagonally arranged holes and rods and rectangular appearing staircaselike features shown in Fig. 1(d). In addition, we observed a number of other seemingly dissimilar peculiar domains, including cubic holes perforating a cuticular scaffolding along with branchlike features. To gain detailed insights into this elaborate structure and to determine whether the aggregate structure consists of domains of the same crystal lattice—oriented differently throughout—or of domains with different crystal lattices altogether, we investigated the intrascale structure by sequential focused ion beam (FIB) milling combined with SEM imaging [17] using a Nova 200 Nanolab dual-beam FIB (gallium liquid metal source)/SEM. In detail, after a few presectioning steps [18], serial sectioning was performed by consecutively milling away ∼30 nm sections of the structure using an ion beam current of 98 pA and 30 kV accelerating voltage. After each milling step, the freshly exposed cross-sectional 2D view of the structure was imaged by SEM. This resulted in a 3D data set consisting of a series or "stack" of 2D SEM images, each with a "thickness" of ∼30 nm—significantly less than the periodicity of the struc-

_____

*Author to whom correspondence should be addressed: bartl@chem.utah.edu
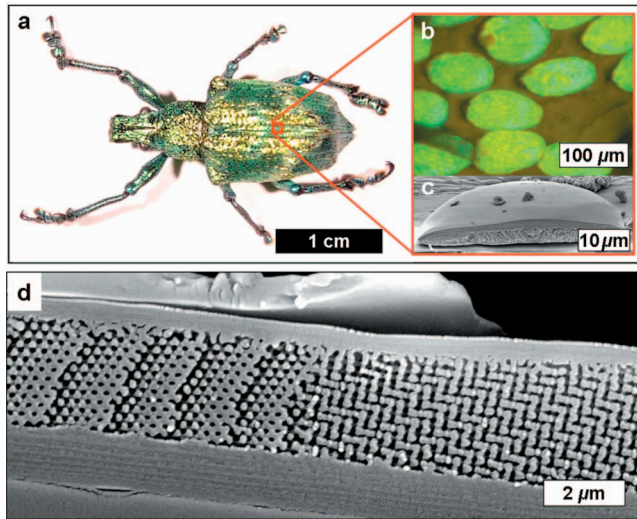
FIG. 1. (Color) (a) Photograph of the weevil *L. augustus*. (b) Optical micrograph of individual scales attached to the exoskeleton of *L. augustus* under white-light illumination. (c) Cross-sectional SEM image of a single scale. (d) Detailed cross-sectional SEM image of a region of a scale.

ture (~300 nm)—yielding an approximately tenfold higher resolution as compared to conventional serial sectioning methods [19]. The obtained series of consecutive SEM images was preprocessed using IMAGEJ [20,21]. Briefly, a smoothing filter was used to reduce noise from the images and a recursive algorithm was applied to align the images of a given stack to one another. The preprocessed stack was imported into the SCIRUN visualization package [22] for volume rendering [Fig. 2(a)]. High-resolution structural information could be obtained by comparing and analyzing a large number of oblique "cuts" through the rendered volume. During this process, we found that the same structural features were present in all of the domains, confirming that individual scales consist of differently oriented single-crystalline domains of the same 3D crystal lattice.

Detailed structural analysis revealed a 3D structure of ABC stacked layers of hexagonally ordered air cylinders in a surrounding cuticular matrix very similar in configuration to a synthetic diamond-based structure proposed [6] and fabricated by Johnson and Joannopoulos for the infrared [10]. Additional quantitative information was obtained from analyzing different structural features of microtomed cross-sectional SEM images. Quantitative structural information was obtained by sampling over a large number of regions within individual scales and between scales from different areas of the beetle's exoskeleton, yielding an average radius and height of the air cylinders of 0.20 and 0.77, respectively, in units of the lattice constant, which was determined to be on average 450 nm (with a 10–20 % variation of structural dimensions). Using the evaluated structural parameters and a dielectric constant of $\varepsilon = 2.50$ for cuticular material [23], we calculated the dielectric function and the band-structure diagram of the beetle's photonic crystal using the MIT Photonics-Band package [24]. Figure 2(b) shows a 3D model of the dielectric function for which the orientation was chosen to reflect the prominent features observed in cross-
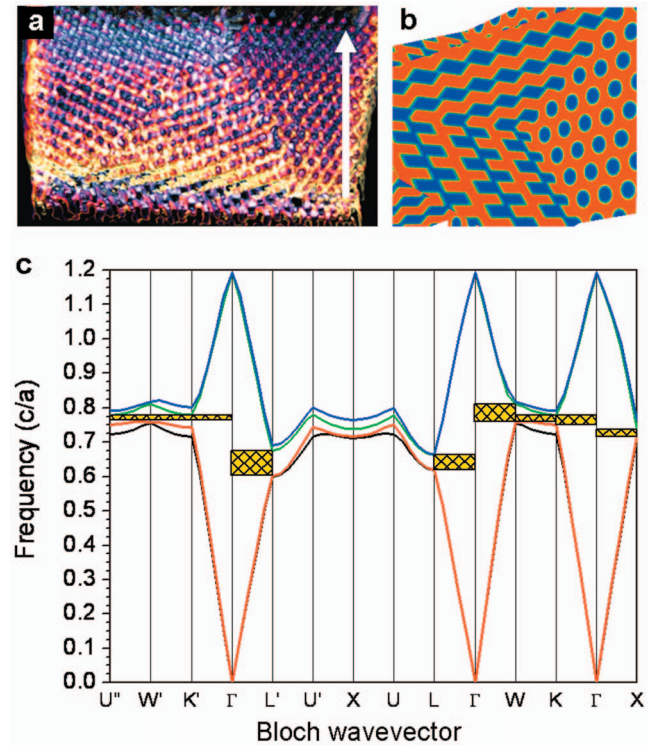
FIG. 2. (Color) (a) Computer-generated 3D reconstruction of serial sectioned data from the FIB milling/SEM imaging process. The arrow indicates the direction of the FIB milling process. (b) Dielectric function of the beetle's photonic crystal generated from 3D structure analysis showing three orthogonal planes. Air: blue; dielectric: red. (c) Photonic band diagram of the beetle diamond-based structure. Stop gaps are denoted by yellow rectangles.

sectional SEM images, such as the hexagonally ordered hole array and the staircaselike pattern. The corresponding photonic band-structure diagram is presented in Fig. 2(c). The most striking feature is that despite the relatively low dielectric constant of cuticular material, calculations reveal a remarkable proximity and overlap of the three stop gaps in the Γ-W (210), Γ-K (110), and Γ-X (100) directions—a direct result of the excellent photonic properties of diamond-based structures. In fact, the cumulative gap of the Γ-W, Γ-K, and Γ-X directions spans the entire green wavelength region. As given in Fig. 2(c), the midgap frequencies are 0.79, 0.77, and 0.73 along the Γ-W, Γ-K, or Γ-X directions, respectively. These frequency values, when normalized within the range of the evaluated average lattice constant (450 nm), yield wavelength ranges between 541–598, 555–614, and 586–647 nm along these directions, respectively.

To test whether the observed near-angle independent green iridescence is the cumulative result of these three single stop bands, we recorded a series of reflectance spectra of small—~7 μm in diameter—different subsections of individual scales [25]. Representative spectra from a single scale are given in Fig. 3 and clearly demonstrate that the broad reflectance peak in fact is composed of three subbands, whose deconvoluted maxima [Figs. 3(b) and 3(c)] coincide well with the midgap location ranges of the calculated Γ-W, Γ-K, and Γ-X stop gaps. As can also be seen in Fig. 3, the
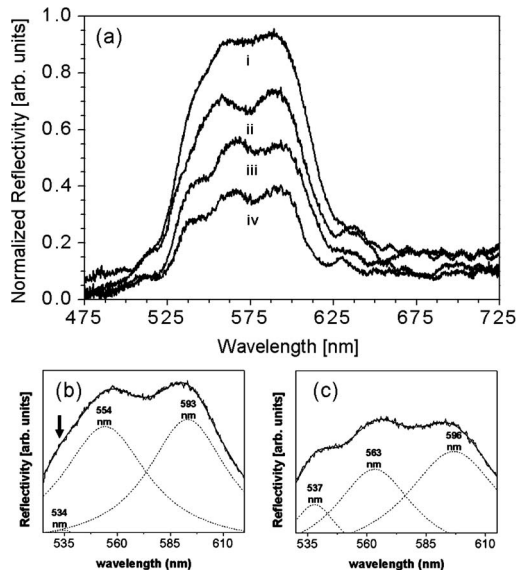
FIG. 3. (a) Normal-incidence reflectance spectra of a single scale (i) and of different ∼7 μm subsections of the same scale (ii)–(iv). (b) and (c) Deconvolution of the high-resolution reflectance peak (full line spectrum) into three major features (dotted line spectra) for plot (ii) (the arrow indicates the shoulder at the Γ-W position) and plot (iii), respectively.

FIG. 4. (a) SEM image of a scale's top surface exposed by FIB milling. (b)–(d) SEM images of individual single-crystalline Γ-W, Γ-K, and Γ-X oriented domains indicated in (a) with corresponding calculated dielectric functions (black-framed insets).

relative intensities of the subbands varied with position, especially in Fig. 3(b), where the lower wavelength feature (Γ-W stop gap) is reduced to a shoulder. We observed this general trend over many different scales, and in each case this cluster of three features was apparent with the deconvoluted peak maxima correlating well with the band-structure calculations.

The excellent agreement between the optical data and our theoretical model is also supported by SEM imaging of the top surface of scales after removal of the structureless top layer using FIB milling. By comparing the exposed domains of the scale's diamond-based structure (Fig. 4) with 2D representations of the calculated dielectric function along the main crystal axes, we found that, in general, the individual single-crystalline domains are oriented with their Γ-W, Γ-K, or Γ-X crystal axes normal or slightly off-normal to the scale top surface. A detailed comparison is shown in Figs. 4(b)–4(d), where the calculated dielectric function of the Γ-W, Γ-K, or Γ-X faces is superimposed over the corresponding domains in the SEM images, demonstrating excellent agreement in the structural characteristics. Furthermore, the considerable variation in the intensity of the Γ-W directional reflection band with spatial position can be accounted for by the general observation from our structural analysis that this crystal axis is featured less frequently normal to the

surface. The prevalence of numerous domains oriented at oblique angles suggests that the orientation of the single crystalline domains is normal to the curved surface of the structureless shell, rather than parallel relative to one another. This sophisticated microdomain orientation of the diamond-based photonic structure gives an overall impression of angle-independent reflection of a broad selective wavelength range, resulting in the spectacular green iridescent coloration of *L. augustus*.

To conclude, by employing sequential ∼30 nm sectioning using a combination of FIB milling and SEM imaging of a natural photonic crystal found in the weevil *L. augustus*, we were able to create a 3D structural reconstruction of previously unachieved resolution. This detailed analysis revealed that the structure of these natural photonic crystals is based on the diamond lattice—the champion of photonic crystal structures. The demonstrated presence of natural diamond-based photonic crystals operating in the visible—a structure that does not yet exist artificially—reflects the ingenuity of photonic structure engineering in biological systems and opens exciting opportunities for advanced optical materials design through new biomimetic manufacturing routes [16].

[1] S. John, Phys. Rev. Lett. **58**, 2486 (1987).

[2] E. Yablonovitch, Phys. Rev. Lett. **58**, 2059 (1987).

[3] J. D. Joannopoulos, P. R. Villeneuve, and S. H. Fan, Nature **386**, 143 (1997).

[4] For a review, see *Photonic Crystals and Light Localization in the 21st Century*, edited by C. M. Soukoulis, NATO Science Series C: Mathematical and Physical Sciences (Kluwer Academic, Dordrecht, 2001).

[5] For a review, see M. Maldovan and E. L. Thomas, Nat. Mater. **3**, 593 (2004), and references therein.

[6] S. G. Johnson and J. D. Joannopoulos, Appl. Phys. Lett. **77**, 3490 (2000).

[7] T. T. Ngo, C. M. Liddell, M. Ghebrebrhan, and J. D. Joannopoulos, Appl. Phys. Lett. **88**, 241920 (2006).

[8] A. P. Hynninen, J. H. J. Thijssen, E. C. M Vermolen, M. Dijkstra, and A. Van Blaaderen, Nat. Mater. **6**, 202 (2007).

[9] M. Maldovan, E. L. Thomas, and C. W. Carter, Appl. Phys. Lett. **84**, 362 (2004).

[10] M. H. Qi, E. Lidorikis, P. T. Rakich, S. G. Johnson, J. D. Joannopoulos, E. P. Ippen, and H. I. Smith, Nature **429**, 538 (2004).

[11] S. Wong, M. Deubel, F. Perez-Willard, S. John, G. A. Ozin, M. Wegener, and G. von Freymann, Adv. Math. **18**, 265 (2006).

[12] F. García-Santamaría, M. Xu, V. Lousse, S. Fan, P. V. Braun, and J. A. Lewis, Adv. Math. **19**, 1567 (2007).

[13] H. Ghiradella, Appl. Opt. **30**, 3492 (1991).

[14] V. Welch, V. Lousse, O. Deparis, A. Parker, and J. P. Vigneron, Phys. Rev. E **75**, 041919 (2007).

[15] P. Vukusic and J. R. Sambles, Nature **424**, 852 (2003).

[16] A. R. Parker and H. E. Townley, Nat. Nanotechnol. **2**, 347 (2007).

[17] M. A. Groeber, B. K. Haley, M. D. Uchic, D. M. Dimiduk, and S. Ghosh, Mater. Charact. **57**, 259 (2006).

[18] To prepare the sample for serial sectioning, a cross-sectional cut was first made by FIB milling to expose the internal structure, followed by milling fiduciary trenches to either side of the selected region to relieve crystal strain during the sectioning process. Finally, the structureless top surface of the scales was removed.

[19] A. Argyros, S. Manos, M. C. J. Large, D. R. McKenzie, G. C. Cox, and D. M. Dwarte, Micron **33**, 483 (2002).

[20] M. D. Abramoff, P. J. Magelhaes, and S. J. Ram, Biophotonics Int. **11**, 36 (2004).

[21] P. Thévenaz, U. E. Ruttimann, and M. Unser, IEEE Trans. Image Process. **7**, 27 (1998).

[22] D. M. Weinstein, S. G. Parker, J. Simpson, K. Zimmerman, and G. Jones, in *The Visualization Handbook*, edited by C. D. Hansen and C. R. Johnson (Elsevier, Burlington, 2005), p. 615.

[23] J. A. Noyes, P. Vukusic, and I. R. Hooper, Opt. Express **15**, 4351 (2007).

[24] S. G. Johnson and J. D. Joannopoulos, Opt. Express **8**, 173 (2001).

[25] Optical reflectance data were collected using a modified Nikon ME600 light microscope with a 20× Nikon objective (numerical aperture of 0.45) and a fiber-coupled Ocean Optics USB4000 vis/NIR spectrometer. An adjustable iris (1–5 mm) or a 200 μm pinhole was used in the image plane of the optical path to isolate a single scale or to reduce the spot size to ~7 μm, respectively.